

First observations of $h_c \rightarrow \text{hadrons}$

M. Ablikim¹, M. N. Achasov^{10,d}, S. Ahmed¹⁵, M. Albrecht⁴, M. Alekseev^{55A,55C}, A. Amoroso^{55A,55C},
F. F. An¹, Q. An^{52,42}, J. Z. Bai¹, Y. Bai⁴¹, O. Bakina²⁷, R. Baldini Ferroli^{23A}, Y. Ban³⁵, K. Begzsuren²⁵,
D. W. Bennett²², J. V. Bennett⁵, N. Berger²⁶, M. Bertani^{23A}, D. Bettoni^{24A}, F. Bianchi^{55A,55C},
E. Boger^{27,b}, I. Boyko²⁷, R. A. Briere⁵, H. Cai⁵⁷, X. Cai^{1,42}, O. Cakir^{45A}, A. Calcaterra^{23A}, G. F. Cao^{1,46},
S. A. Cetin^{45B}, J. Chai^{55C}, J. F. Chang^{1,42}, G. Chelkov^{27,b,c}, G. Chen¹, H. S. Chen^{1,46}, J. C. Chen¹,
M. L. Chen^{1,42}, P. L. Chen⁵³, S. J. Chen³³, X. R. Chen³⁰, Y. B. Chen^{1,42}, W. Cheng^{55C}, X. K. Chu³⁵,
G. Cibinetto^{24A}, F. Cossio^{55C}, H. L. Dai^{1,42}, J. P. Dai^{37,h}, A. Dbeyssi¹⁵, D. Dedovich²⁷, Z. Y. Deng¹,
A. Denig²⁶, I. Denysenko²⁷, M. Destefanis^{55A,55C}, F. De Mori^{55A,55C}, Y. Ding³¹, C. Dong³⁴, J. Dong^{1,42},
L. Y. Dong^{1,46}, M. Y. Dong^{1,42,46}, Z. L. Dou³³, S. X. Du⁶⁰, P. F. Duan¹, J. Fang^{1,42}, S. S. Fang^{1,46},
Y. Fang¹, R. Farinelli^{24A,24B}, L. Fava^{55B,55C}, S. Fegan²⁶, F. Feldbauer⁴, G. Felici^{23A}, C. Q. Feng^{52,42},
E. Fioravanti^{24A}, M. Fritsch⁴, C. D. Fu¹, Q. Gao¹, X. L. Gao^{52,42}, Y. Gao⁴⁴, Y. G. Gao⁶, Z. Gao^{52,42}, B.
Garillon²⁶, I. Garzia^{24A}, A. Gilman⁴⁹, K. Goetzen¹¹, L. Gong³⁴, W. X. Gong^{1,42}, W. Gradl²⁶,
M. Greco^{55A,55C}, L. M. Gu³³, M. H. Gu^{1,42}, Y. T. Gu¹³, A. Q. Guo¹, L. B. Guo³², R. P. Guo^{1,46},
Y. P. Guo²⁶, A. Guskov²⁷, Z. Haddadi²⁹, S. Han⁵⁷, X. Q. Hao¹⁶, F. A. Harris⁴⁷, K. L. He^{1,46}, X. Q. He⁵¹,
F. H. Heinsius⁴, T. Held⁴, Y. K. Heng^{1,42,46}, Z. L. Hou¹, H. M. Hu^{1,46}, J. F. Hu^{37,h}, T. Hu^{1,42,46}, Y. Hu¹,
G. S. Huang^{52,42}, J. S. Huang¹⁶, X. T. Huang³⁶, X. Z. Huang³³, Z. L. Huang³¹, T. Hussain⁵⁴, W. Ikegami
Andersson⁵⁶, M. Irshad^{52,42}, Q. Ji¹, Q. P. Ji¹⁶, X. B. Ji^{1,46}, X. L. Ji^{1,42}, X. S. Jiang^{1,42,46}, X. Y. Jiang³⁴,
J. B. Jiao³⁶, Z. Jiao¹⁸, D. P. Jin^{1,42,46}, S. Jin^{1,46}, Y. Jin⁴⁸, T. Johansson⁵⁶, A. Julin⁴⁹,
N. Kalantar-Nayestanaki²⁹, X. S. Kang³⁴, M. Kavatsyuk²⁹, B. C. Ke¹, I. K. Keshk⁴, T. Khan^{52,42},
A. Khoukaz⁵⁰, P. Kiese²⁶, R. Kiuchi¹, R. Kliemt¹¹, L. Koch²⁸, O. B. Kolcu^{45B,f}, B. Kopf⁴,
M. Kornicer⁴⁷, M. Kuemmel⁴, M. Kuessner⁴, A. Kupsc⁵⁶, M. Kurth¹, W. Kühn²⁸, J. S. Lange²⁸, P.
Larin¹⁵, L. Lavezzi^{55C}, S. Leiber⁴, H. Leithoff²⁶, C. Li⁵⁶, Cheng Li^{52,42}, D. M. Li⁶⁰, F. Li^{1,42}, F. Y. Li³⁵,
G. Li¹, H. B. Li^{1,46}, H. J. Li^{1,46}, J. C. Li¹, J. W. Li⁴⁰, K. J. Li⁴³, Kang Li¹⁴, Ke Li¹, Lei Li³, P. L. Li^{52,42},
P. R. Li^{46,7}, Q. Y. Li³⁶, T. Li³⁶, W. D. Li^{1,46}, W. G. Li¹, X. L. Li³⁶, X. N. Li^{1,42}, X. Q. Li³⁴, Z. B. Li⁴³,
H. Liang^{52,42}, Y. F. Liang³⁹, Y. T. Liang²⁸, G. R. Liao¹², L. Z. Liao^{1,46}, J. Libby²¹, C. X. Lin⁴³,
D. X. Lin¹⁵, B. Liu^{37,h}, B. J. Liu¹, C. X. Liu¹, D. Liu^{52,42}, D. Y. Liu^{37,h}, F. H. Liu³⁸, Fang Liu¹,
Feng Liu⁶, H. B. Liu¹³, H. L. Liu⁴¹, H. M. Liu^{1,46}, Huanhuan Liu¹, Huihui Liu¹⁷, J. B. Liu^{52,42},
J. Y. Liu^{1,46}, K. Liu⁴⁴, K. Y. Liu³¹, Ke Liu⁶, L. D. Liu³⁵, Q. Liu⁴⁶, S. B. Liu^{52,42}, X. Liu³⁰, Y. B. Liu³⁴,
Z. A. Liu^{1,42,46}, Zhiqing Liu²⁶, Y. F. Long³⁵, X. C. Lou^{1,42,46}, H. J. Lu¹⁸, J. G. Lu^{1,42}, Y. Lu¹,

Y. P. Lu^{1,42}, C. L. Luo³², M. X. Luo⁵⁹, T. Luo^{9,j}, X. L. Luo^{1,42}, S. Lusso^{55C}, X. R. Lyu⁴⁶, F. C. Ma³¹,
 H. L. Ma¹, L. L. Ma³⁶, M. M. Ma^{1,46}, Q. M. Ma¹, T. Ma¹, X. N. Ma³⁴, X. Y. Ma^{1,42}, Y. M. Ma³⁶,
 F. E. Maas¹⁵, M. Maggiora^{55A,55C}, S. Maldaner²⁶, Q. A. Malik⁵⁴, A. Mangoni^{23B}, Y. J. Mao³⁵,
 Z. P. Mao¹, S. Marcello^{55A,55C}, Z. X. Meng⁴⁸, J. G. Messchendorp²⁹, G. Mezzadri^{24B}, J. Min^{1,42},
 T. J. Min³³, R. E. Mitchell²², X. H. Mo^{1,42,46}, Y. J. Mo⁶, C. Morales Morales¹⁵, N. Yu. Muchnoi^{10,d},
 H. Muramatsu⁴⁹, A. Mustafa⁴, Y. Nefedov²⁷, F. Nerling¹¹, I. B. Nikolaev^{10,d}, Z. Ning^{1,42}, S. Nisar⁸,
 S. L. Niu^{1,42}, X. Y. Niu^{1,46}, S. L. Olsen⁴⁶, Q. Ouyang^{1,42,46}, S. Pacetti^{23B}, Y. Pan^{52,42}, M. Papenbrock⁵⁶,
 P. Patteri^{23A}, M. Pelizaeus⁴, J. Pellegrino^{55A,55C}, H. P. Peng^{52,42}, Z. Y. Peng¹³, K. Peters^{11,g},
 J. Pettersson⁵⁶, J. L. Ping³², R. G. Ping^{1,46}, A. Pitka⁴, R. Poling⁴⁹, V. Prasad^{52,42}, H. R. Qi², M. Qi³³,
 T. Y. Qi², S. Qian^{1,42}, C. F. Qiao⁴⁶, N. Qin⁵⁷, X. S. Qin⁴, Z. H. Qin^{1,42}, J. F. Qiu¹, S. Q. Qu³⁴,
 K. H. Rashid^{54,i}, C. F. Redmer²⁶, M. Richter⁴, M. Ripka²⁶, A. Rivetti^{55C}, M. Rolo^{55C}, G. Rong^{1,46},
 Ch. Rosner¹⁵, A. Sarantsev^{27,e}, M. Savrić^{24B}, K. Schoenning⁵⁶, W. Shan¹⁹, X. Y. Shan^{52,42}, M. Shao^{52,42},
 C. P. Shen², P. X. Shen³⁴, X. Y. Shen^{1,46}, H. Y. Sheng¹, X. Shi^{1,42}, J. J. Song³⁶, W. M. Song³⁶,
 X. Y. Song¹, S. Sosio^{55A,55C}, C. Sowa⁴, S. Spataro^{55A,55C}, G. X. Sun¹, J. F. Sun¹⁶, L. Sun⁵⁷,
 S. S. Sun^{1,46}, X. H. Sun¹, Y. J. Sun^{52,42}, Y. K. Sun^{52,42}, Y. Z. Sun¹, Z. J. Sun^{1,42}, Z. T. Sun¹, Y. T. Tan^{52,42},
 C. J. Tang³⁹, G. Y. Tang¹, X. Tang¹, I. Tapan^{45C}, M. Tiemens²⁹, B. Tsednee²⁵, I. Uman^{45D}, B. Wang¹,
 B. L. Wang⁴⁶, C. W. Wang³³, D. Wang³⁵, D. Y. Wang³⁵, Dan Wang⁴⁶, K. Wang^{1,42}, L. L. Wang¹,
 L. S. Wang¹, M. Wang³⁶, Meng Wang^{1,46}, P. Wang¹, P. L. Wang¹, W. P. Wang^{52,42}, X. F. Wang⁴⁴,
 Y. Wang^{52,42}, Y. F. Wang^{1,42,46}, Z. Wang^{1,42}, Z. G. Wang^{1,42}, Z. Y. Wang¹, Zongyuan Wang^{1,46},
 T. Weber⁴, D. H. Wei¹², P. Weidenkaff²⁶, S. P. Wen¹, U. Wiedner⁴, M. Wolke⁵⁶, L. H. Wu¹, L. J. Wu^{1,46},
 Z. Wu^{1,42}, L. Xia^{52,42}, X. Xia³⁶, Y. Xia²⁰, D. Xiao¹, Y. J. Xiao^{1,46}, Z. J. Xiao³², Y. G. Xie^{1,42}, Y. H. Xie⁶,
 X. A. Xiong^{1,46}, Q. L. Xiu^{1,42}, G. F. Xu¹, J. J. Xu^{1,46}, L. Xu¹, Q. J. Xu¹⁴, Q. N. Xu⁴⁶, X. P. Xu⁴⁰,
 F. Yan⁵³, L. Yan^{55A,55C}, W. B. Yan^{52,42}, W. C. Yan², Y. H. Yan²⁰, H. J. Yang^{37,h}, H. X. Yang¹, L. Yang⁵⁷,
 R. X. Yang^{52,42}, Y. H. Yang³³, Y. X. Yang¹², Yifan Yang^{1,46}, Z. Q. Yang²⁰, M. Ye^{1,42}, M. H. Ye⁷,
 J. H. Yin¹, Z. Y. You⁴³, B. X. Yu^{1,42,46}, C. X. Yu³⁴, J. S. Yu³⁰, J. S. Yu²⁰, C. Z. Yuan^{1,46}, Y. Yuan¹,
 A. Yuncu^{45B,a}, A. A. Zafar⁵⁴, Y. Zeng²⁰, B. X. Zhang¹, B. Y. Zhang^{1,42}, C. C. Zhang¹, D. H. Zhang¹,
 H. H. Zhang⁴³, H. Y. Zhang^{1,42}, J. Zhang^{1,46}, J. L. Zhang⁵⁸, J. Q. Zhang⁴, J. W. Zhang^{1,42,46}, J. Y. Zhang¹,
 J. Z. Zhang^{1,46}, K. Zhang^{1,46}, L. Zhang⁴⁴, S. F. Zhang³³, T. J. Zhang^{37,h}, X. Y. Zhang³⁶, Y. Zhang^{52,42},
 Y. H. Zhang^{1,42}, Y. T. Zhang^{52,42}, Yang Zhang¹, Yao Zhang¹, Yu Zhang⁴⁶, Z. H. Zhang⁶, Z. P. Zhang⁵²,
 Z. Y. Zhang⁵⁷, G. Zhao¹, J. W. Zhao^{1,42}, J. Y. Zhao^{1,46}, J. Z. Zhao^{1,42}, Lei Zhao^{52,42}, Ling Zhao¹,
 M. G. Zhao³⁴, Q. Zhao¹, S. J. Zhao⁶⁰, T. C. Zhao¹, Y. B. Zhao^{1,42}, Z. G. Zhao^{52,42}, A. Zhemchugov^{27,b},

B. Zheng⁵³, J. P. Zheng^{1,42}, W. J. Zheng³⁶, Y. H. Zheng⁴⁶, B. Zhong³², L. Zhou^{1,42}, Q. Zhou^{1,46},
X. Zhou⁵⁷, X. K. Zhou^{52,42}, X. R. Zhou^{52,42}, X. Y. Zhou¹, Xiaoyu Zhou²⁰, Xu Zhou²⁰, A. N. Zhu^{1,46},
J. Zhu³⁴, J. Zhu⁴³, K. Zhu¹, K. J. Zhu^{1,42,46}, S. Zhu¹, S. H. Zhu⁵¹, X. L. Zhu⁴⁴, Y. C. Zhu^{52,42},
Y. S. Zhu^{1,46}, Z. A. Zhu^{1,46}, J. Zhuang^{1,42}, B. S. Zou¹, J. H. Zou¹

(BESIII Collaboration)

¹ *Institute of High Energy Physics, Beijing 100049, People's Republic of China*

² *Beihang University, Beijing 100191, People's Republic of China*

³ *Beijing Institute of Petrochemical Technology, Beijing 102617, People's Republic of China*

⁴ *Bochum Ruhr-University, D-44780 Bochum, Germany*

⁵ *Carnegie Mellon University, Pittsburgh, Pennsylvania 15213, USA*

⁶ *Central China Normal University, Wuhan 430079, People's Republic of China*

⁷ *China Center of Advanced Science and Technology, Beijing 100190, People's Republic of China*

⁸ *COMSATS Institute of Information Technology, Lahore, Defence Road, Off Raiwind Road, 54000
Lahore, Pakistan*

⁹ *Fudan University, Shanghai 200443, People's Republic of China*

¹⁰ *G.I. Budker Institute of Nuclear Physics SB RAS (BINP), Novosibirsk 630090, Russia*

¹¹ *GSI Helmholtzcentre for Heavy Ion Research GmbH, D-64291 Darmstadt, Germany*

¹² *Guangxi Normal University, Guilin 541004, People's Republic of China*

¹³ *Guangxi University, Nanning 530004, People's Republic of China*

¹⁴ *Hangzhou Normal University, Hangzhou 310036, People's Republic of China*

¹⁵ *Helmholtz Institute Mainz, Johann-Joachim-Becher-Weg 45, D-55099 Mainz, Germany*

¹⁶ *Henan Normal University, Xinxiang 453007, People's Republic of China*

¹⁷ *Henan University of Science and Technology, Luoyang 471003, People's Republic of China*

¹⁸ *Huangshan College, Huangshan 245000, People's Republic of China*

¹⁹ *Hunan Normal University, Changsha 410081, People's Republic of China*

²⁰ *Hunan University, Changsha 410082, People's Republic of China*

²¹ *Indian Institute of Technology Madras, Chennai 600036, India*

²² *Indiana University, Bloomington, Indiana 47405, USA*

²³ (A) *INFN Laboratori Nazionali di Frascati, I-00044, Frascati, Italy*; (B) *INFN and University of Perugia,
I-06100, Perugia, Italy*

- ²⁴ (A)INFN Sezione di Ferrara, I-44122, Ferrara, Italy; (B)University of Ferrara, I-44122, Ferrara, Italy
- ²⁵ Institute of Physics and Technology, Peace Ave. 54B, Ulaanbaatar 13330, Mongolia
- ²⁶ Johannes Gutenberg University of Mainz, Johann-Joachim-Becher-Weg 45, D-55099 Mainz, Germany
- ²⁷ Joint Institute for Nuclear Research, 141980 Dubna, Moscow region, Russia
- ²⁸ Justus-Liebig-Universitaet Giessen, II. Physikalisches Institut, Heinrich-Buff-Ring 16, D-35392 Giessen, Germany
- ²⁹ KVI-CART, University of Groningen, NL-9747 AA Groningen, The Netherlands
- ³⁰ Lanzhou University, Lanzhou 730000, People's Republic of China
- ³¹ Liaoning University, Shenyang 110036, People's Republic of China
- ³² Nanjing Normal University, Nanjing 210023, People's Republic of China
- ³³ Nanjing University, Nanjing 210093, People's Republic of China
- ³⁴ Nankai University, Tianjin 300071, People's Republic of China
- ³⁵ Peking University, Beijing 100871, People's Republic of China
- ³⁶ Shandong University, Jinan 250100, People's Republic of China
- ³⁷ Shanghai Jiao Tong University, Shanghai 200240, People's Republic of China
- ³⁸ Shanxi University, Taiyuan 030006, People's Republic of China
- ³⁹ Sichuan University, Chengdu 610064, People's Republic of China
- ⁴⁰ Soochow University, Suzhou 215006, People's Republic of China
- ⁴¹ Southeast University, Nanjing 211100, People's Republic of China
- ⁴² State Key Laboratory of Particle Detection and Electronics, Beijing 100049, Hefei 230026, People's Republic of China
- ⁴³ Sun Yat-Sen University, Guangzhou 510275, People's Republic of China
- ⁴⁴ Tsinghua University, Beijing 100084, People's Republic of China
- ⁴⁵ (A)Ankara University, 06100 Tandogan, Ankara, Turkey; (B)Istanbul Bilgi University, 34060 Eyup, Istanbul, Turkey; (C)Uludag University, 16059 Bursa, Turkey; (D)Near East University, Nicosia, North Cyprus, Mersin 10, Turkey
- ⁴⁶ University of Chinese Academy of Sciences, Beijing 100049, People's Republic of China
- ⁴⁷ University of Hawaii, Honolulu, Hawaii 96822, USA
- ⁴⁸ University of Jinan, Jinan 250022, People's Republic of China
- ⁴⁹ University of Minnesota, Minneapolis, Minnesota 55455, USA
- ⁵⁰ University of Muenster, Wilhelm-Klemm-Str. 9, 48149 Muenster, Germany

- ⁵¹ *University of Science and Technology Liaoning, Anshan 114051, People's Republic of China*
- ⁵² *University of Science and Technology of China, Hefei 230026, People's Republic of China*
- ⁵³ *University of South China, Hengyang 421001, People's Republic of China*
- ⁵⁴ *University of the Punjab, Lahore-54590, Pakistan*
- ⁵⁵ (A)*University of Turin, I-10125, Turin, Italy; (B)University of Eastern Piedmont, I-15121, Alessandria, Italy; (C)INFN, I-10125, Turin, Italy*
- ⁵⁶ *Uppsala University, Box 516, SE-75120 Uppsala, Sweden*
- ⁵⁷ *Wuhan University, Wuhan 430072, People's Republic of China*
- ⁵⁸ *Xinyang Normal University, Xinyang 464000, People's Republic of China*
- ⁵⁹ *Zhejiang University, Hangzhou 310027, People's Republic of China*
- ⁶⁰ *Zhengzhou University, Zhengzhou 450001, People's Republic of China*
- ^a *Also at Bogazici University, 34342 Istanbul, Turkey*
- ^b *Also at the Moscow Institute of Physics and Technology, Moscow 141700, Russia*
- ^c *Also at the Functional Electronics Laboratory, Tomsk State University, Tomsk, 634050, Russia*
- ^d *Also at the Novosibirsk State University, Novosibirsk, 630090, Russia*
- ^e *Also at the NRC "Kurchatov Institute", PNPI, 188300, Gatchina, Russia*
- ^f *Also at Istanbul Arel University, 34295 Istanbul, Turkey*
- ^g *Also at Goethe University Frankfurt, 60323 Frankfurt am Main, Germany*
- ^h *Also at Key Laboratory for Particle Physics, Astrophysics and Cosmology, Ministry of Education; Shanghai Key Laboratory for Particle Physics and Cosmology; Institute of Nuclear and Particle Physics, Shanghai 200240, People's Republic of China*
- ⁱ *Government College Women University, Sialkot - 51310. Punjab, Pakistan.*
- ^j *Key Laboratory of Nuclear Physics and Ion-beam Application (MOE) and Institute of Modern Physics, Fudan University, Shanghai 200443, People's Republic of China*

(Dated: October 30, 2018)

Abstract

Based on $(4.48 \pm 0.03) \times 10^8$ $\psi(3686)$ events collected with the BESIII detector, five h_c hadronic decays are searched for via process $\psi(3686) \rightarrow \pi^0 h_c$. Three of them, $h_c \rightarrow p\bar{p}\pi^+\pi^-$, $\pi^+\pi^-\pi^0$, and $2(\pi^+\pi^-)\pi^0$ are observed for the first time, with statistical significances of 7.4σ , 4.9σ , and 9.1σ , and branching fractions of $(2.89 \pm 0.32 \pm 0.55) \times 10^{-3}$, $(1.60 \pm 0.40 \pm 0.32) \times 10^{-3}$, and $(7.44 \pm 0.94 \pm 1.56) \times 10^{-3}$, respectively, where the first uncertainties are statistical and the second systematic. No significant signal is observed for the other two decay modes, and the corresponding upper limits of the branching fractions are determined to be $\mathcal{B}(h_c \rightarrow 3(\pi^+\pi^-)\pi^0) < 8.7 \times 10^{-3}$ and $\mathcal{B}(h_c \rightarrow K^+K^-\pi^+\pi^-) < 5.8 \times 10^{-4}$ at 90% confidence level.

PACS numbers: 13.30.Eg, 13.25.Gv, 14.40.Lb

The study of charmonium states is crucial to reach a deeper understanding of the low-energy regime of quantum chromodynamics (QCD), a theory describing the strong interaction and has been tested successfully in the high-energy regime. However, the measurements of the decays of spin singlet charmonium state $h_c(^1P_1)$ have remained sparse despite of its discovery in 2005 [1, 2]. Its best-measured decay is the radiative transition $h_c \rightarrow \gamma\eta_c$ [3–5], while the sum of the other known h_c decay branching fractions is less than 3% [6]. Among those measurements, there is only one evidence for h_c hadronic decays, $h_c \rightarrow 2(\pi^+\pi^-)\pi^0$, which is reported by CLEO-c with a statistical significance of 4.4σ [7]. Improved measurement and observation of new h_c hadronic decay modes will shed light on the understanding of the h_c decay mechanism, and be helpful for guiding the development of QCD based models. For example, the perturbative QCD (pQCD) and non-relativistic QCD (NRQCD) are the two competitive models to describe the low-energy QCD features, and their predicted ratios of the hadronic widths of h_c to η_c ($\Gamma_{h_c}^{\text{had}}/\Gamma_{\eta_c}^{\text{had}}$) are very different [8], as well as h_c to J/ψ ($\Gamma_{h_c}^{\text{had}}/\Gamma_{J/\psi}^{\text{had}}$). With new measurements of h_c hadronic decays, the ratios of widths for the exclusive channels can be achieved and compared with theoretical calculation to check which model is favored. At present, a large $\psi(3686)$ sample with 4.48×10^8 events [9] has been collected with the BESIII detector, which enables us to study h_c decays. In this Letter, we report the first observations of decays $h_c \rightarrow p\bar{p}\pi^+\pi^-$, $\pi^+\pi^-\pi^0$, and $2(\pi^+\pi^-)\pi^0$, and the upper limits of decays $h_c \rightarrow 3(\pi^+\pi^-)\pi^0$ and $K^+K^-\pi^+\pi^-$.

The BESIII detector [10] is a general purpose detector with a 93% solid angle coverage. A small-cell helium-based multi-layer drift chamber (MDC) determines the momentum of charged particles in a 1 T magnetic field with a resolution of 0.5% at 1 GeV/c, and measures their ionization energy loss (dE/dx) with resolutions better than 6%. A CsI(Tl) electromagnetic calorimeter (EMC) measures the photon energies with resolutions 2.5% (5.0%) in the barrel (end caps). A time-of-flight system (TOF), composed of plastic scintillators with resolution of 80 ps (110 ps) in the barrel (end caps), is used for particle identification (PID). A resistive plate chambers based muon counter (MUC) with 2 cm position resolution is used for muon identification.

To obtain the detection efficiencies, the signal Monte Carlo (MC) samples for the processes $\psi(3686) \rightarrow \pi^0 h_c$, and $h_c \rightarrow p\bar{p}\pi^+\pi^-$, $\pi^+\pi^-\pi^0$, $2(\pi^+\pi^-)\pi^0$, $3(\pi^+\pi^-)\pi^0$, or $K^+K^-\pi^+\pi^-$ are generated based on the phase space (PHSP) distributions. To investigate the background, an inclusive MC sample of 5.06×10^8 $\psi(3686)$ events is generated, in which the $\psi(3686)$ resonance is produced with KKMC [11, 12]. The decays with known branching fractions obtained from the Particle Data Group (PDG) [6] are generated with EVTGEN [13], while the unknown decays are

generated with LUNDCHARM [14]. In all the simulations, the GEANT4-based [15, 16] package BOOST [17] is used to model the detector responses and incorporate time-dependent beam backgrounds.

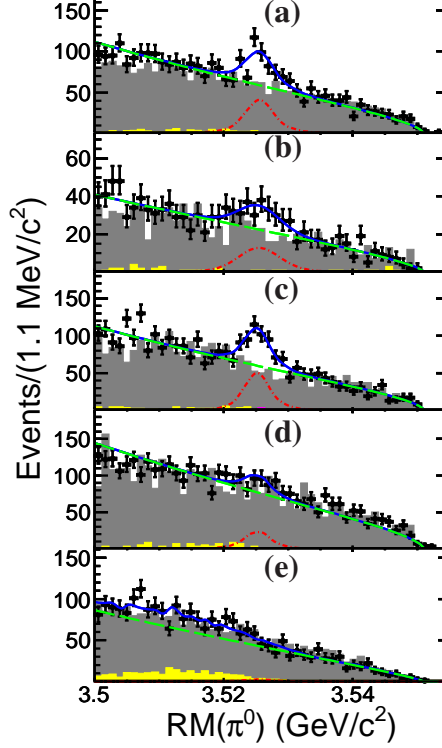


FIG. 1. Recoiling mass spectra of π^0 for decays $\psi(3686) \rightarrow \pi^0 h_c$ with $h_c \rightarrow p\bar{p}\pi^+\pi^-$ (a), $h_c \rightarrow \pi^+\pi^-\pi^0$ (b), $h_c \rightarrow 2(\pi^+\pi^-)\pi^0$ (c), $h_c \rightarrow 3(\pi^+\pi^-)\pi^0$ (d), and $h_c \rightarrow K^+K^-\pi^+\pi^-$ (e), where π^0 is the one with lower energy for $\psi(3686) \rightarrow \pi^0 h_c$ with $h_c \rightarrow n(\pi^+\pi^-)\pi^0$ ($n = 1, 2, 3$). In each spectrum, the dots with error bars represent data, the yellow shaded histogram is the background process $\psi(3686) \rightarrow \gamma\chi_{c2}$, the pink filled histogram is the background process $\psi(3686) \rightarrow \pi^0 h_c$, $h_c \rightarrow \gamma\eta_c$, the grey filled histogram is the background from inclusive MC, the green dashed curve is the fitted background, the red dash-dot curve is the fitted signal, and the blue curve is the fitted result (color online).

Events with expected number of charged particle candidates and at least two photon candidates for $h_c \rightarrow p\bar{p}\pi^+\pi^-$, $K^+K^-\pi^+\pi^-$ modes or four for $h_c \rightarrow n(\pi^+\pi^-)\pi^0$ ($n = 1, 2, 3$) modes are selected. Each charged track reconstructed in the MDC is required to be within 10 cm of interaction point along the beam direction and 1 cm in the plane perpendicular to the beam. The polar angle θ of the tracks must be within the fiducial volume of the MDC ($|\cos\theta| < 0.93$). The TOF and dE/dx information of each charged track is used to calculate the corresponding probabilities of the hypotheses that a track is a pion, kaon or proton for particle identification. Electromagnetic showers are reconstructed by clustering energies deposited in the EMC, and in the nearby TOF counters. A photon candidate is such a shower with a deposited energy larger than 25

MeV in the barrel region ($|\cos\theta| < 0.8$) or 50 MeV in the end cap region ($0.86 < |\cos\theta| < 0.92$). The time t from the EMC is required to be $0 < t < 700$ ns to suppress electronic noise and beam-associated background. The angle between photon and the extrapolated impact point in the EMC of the nearest charged tracks must be larger than 10° for pion and 20° for proton, respectively, to make sure that the cluster is not from a charged track.

After a vertex fit constraining all the charged tracks from a common interaction point is applied, a kinematic fit is performed to further improve resolution and suppress background. In the kinematic fit, the constraints on the four-momentum conservation between initial and final states, and the $\gamma\gamma$ invariant mass ($0.107 < M(\gamma\gamma) < 0.163$ GeV/ c^2) to be the nominal π^0 mass [6] are taken into account. The photons are looped over to make combinations with the charged tracks if more than the required number of photons are reconstructed in an event, and the combination with the smallest χ^2 is kept. The χ^2 is required to be less than a specific value determined by maximizing $S/\sqrt{S+B}$, which is considered as figure of merit (FOM). Here, S is the number of signal events from MC simulation normalized to the preliminary result measured with the un-optimized selection criteria and B is the number of background events extracted from the inclusive MC sample. The FOM is maximized in the h_c signal region $|RM(\pi_l^0) - 3.525| < 0.008$ GeV/ c^2 , where $RM(\pi_l^0)$ is the recoiling mass of π^0 (lower energy one in case of multiple π^0 s in an event).

To suppress the background with different numbers of photons as in signal modes, such as the main background decay $\psi(3686) \rightarrow \gamma\chi_{c2}$ (χ_{c2} decays to the same h_c decay final states), $\chi_{4C,\text{exp}}^2 < \chi_{4C,\text{unexp}}^2$ is required for each decay mode. Here $\chi_{4C,\text{exp}}^2$ is obtained from four-momentum kinematic fit by looping over all the photon candidates to select ones with the expected number of photons for signal, while $\chi_{4C,\text{unexp}}^2$ is obtained by the similar method but with unexpected, more or less, number of photons.

The background contributions from $\psi(3686)$ decays are estimated with the inclusive MC sample. Mass windows for each decay mode, optimized simultaneously with FOM, are required to suppress the corresponding background events, and listed below:

- For $h_c \rightarrow p\bar{p}\pi^+\pi^-$ mode, the mass windows, $|RM(\pi^+\pi^-) - m(J/\psi)| > 18$ MeV/ c^2 , $|M(\pi^+\pi^-\pi^0) - m(\eta)| > 14$ MeV/ c^2 and $|M(\pi^+\pi^-\pi^0) - m(\omega)| > 6$ MeV/ c^2 are required to veto the background contributions from $\psi(3686) \rightarrow \pi^+\pi^-J/\psi$, or events with $\eta \rightarrow \pi^+\pi^-\pi^0$ or $\omega \rightarrow \pi^+\pi^-\pi^0$, where $RM(\pi^+\pi^-)$ is the recoil mass of $\pi^+\pi^-$, and $M(\pi^+\pi^-\pi^0)$ is the invariant mass of $\pi^+\pi^-\pi^0$, while $m(J/\psi)$, $m(\eta)$, and $m(\omega)$ are the nominal masses of J/ψ , η , and ω [6], respectively.

- For $h_c \rightarrow \pi^+\pi^-\pi^0$ mode, the mass windows, $|RM(\pi_l^0\pi_h^0) - m(J/\psi)| > 74 \text{ MeV}/c^2$ and $|RM(\pi_h^0) - m(\omega)| > 32 \text{ MeV}/c^2$, are required to veto the background contributions from $\psi(3686) \rightarrow \pi^0\pi^0 J/\psi$ and $\psi(3686) \rightarrow \pi^0\omega$, where $RM(\pi_l^0\pi_h^0)$ and $RM(\pi_h^0)$ are the recoiling masses of $\pi_l^0\pi_h^0$ and π_h^0 (π_h^0 is π^0 with higher energy), respectively.
- For $h_c \rightarrow 2(\pi^+\pi^-\pi^0)$ mode, the mass windows, $|RM(\pi_l^0\pi_h^0) - m(J/\psi)| > 20 \text{ MeV}/c^2$, $|RM(\pi^+\pi^-) - m(J/\psi)| > 22 \text{ MeV}/c^2$, $|M(\pi^+\pi^-\pi_l^0) - m(\eta)| > 16 \text{ MeV}/c^2$, and $|M(\pi^+\pi^-\pi_l^0) - m(\omega)| > 20 \text{ MeV}/c^2$, are required to veto the background contributions from $\psi(3686) \rightarrow \pi^0\pi^0 J/\psi$, $\psi(3686) \rightarrow \pi^+\pi^- J/\psi$, or events with $\eta \rightarrow \pi^+\pi^-\pi^0$ or $\omega \rightarrow \pi^+\pi^-\pi^0$.
- For $h_c \rightarrow 3(\pi^+\pi^-\pi^0)$ mode, the mass windows, $|RM(\pi_l^0\pi_h^0) - m(J/\psi)| > 18 \text{ MeV}/c^2$, $|RM(\pi^+\pi^-) - m(J/\psi)| > 20 \text{ MeV}/c^2$ and $|M(\pi^+\pi^-\pi_l^0) - m(\eta)| > 16 \text{ MeV}/c^2$, are required to veto the background contributions from $\psi(3686) \rightarrow \pi^0\pi^0 J/\psi$, $\psi(3686) \rightarrow \pi^+\pi^- J/\psi$, or events with $\eta \rightarrow \pi^+\pi^-\pi^0$.
- For $h_c \rightarrow K^+K^-\pi^+\pi^-$ mode, the mass windows, $|RM(\pi^+\pi^-) - m(J/\psi)| > 22 \text{ MeV}/c^2$, $|M(\pi^+\pi^-\pi^0) - m(\eta)| > 16 \text{ MeV}/c^2$ and $|M(\pi^+\pi^-\pi^0) - m(\omega)| > 20 \text{ MeV}/c^2$, are required to veto the background contributions from $\psi(3686) \rightarrow \pi^+\pi^- J/\psi$, $\eta \rightarrow \pi^+\pi^-\pi^0$, or events with $\omega \rightarrow \pi^+\pi^-\pi^0$.

Figure 1 shows the recoiling mass distribution of π_l^0 obtained by applying the above selection criteria. Clear h_c the signal is observed in $h_c \rightarrow p\bar{p}\pi^+\pi^-$, $\pi^+\pi^-\pi^0$, and $2(\pi^+\pi^-\pi^0)$, while no obvious signal is observed for $h_c \rightarrow 3(\pi^+\pi^-\pi^0)$ and $K^+K^-\pi^+\pi^-$. For decay mode $h_c \rightarrow 2(\pi^+\pi^-\pi^0)$, there are $11.0 \pm 3.3 \pm 2.5$ peaking background events from $\psi(3686) \rightarrow \pi^0 h_c (h_c \rightarrow \gamma\eta_c)$, where the first uncertainty is statistical and second systematic, while no peaking background is found for the other decay modes based on inclusive MC. The remaining background from $\psi(3686) \rightarrow \gamma\chi_{c2}$ is negligible for all the decay modes except $h_c \rightarrow K^+K^-\pi^+\pi^-$, therefore, the process $\psi(3686) \rightarrow \gamma\chi_{c2}(\chi_{c2} \rightarrow K^+K^-\pi^+\pi^-)$ will be considered especially for $h_c \rightarrow K^+K^-\pi^+\pi^-$ mode in the fit below. The background contributions from the continuum processes are studied with a 44 pb^{-1} data set taken at $\sqrt{s} = 3.65 \text{ GeV}$. No h_c signal is observed in any of the final states analyzed.

To obtain the number of signal events from $\psi(3686) \rightarrow \pi^0 h_c$ with $h_c \rightarrow p\bar{p}\pi^+\pi^-$, $\pi^+\pi^-\pi^0$, $2(\pi^+\pi^-\pi^0)$, $3(\pi^+\pi^-\pi^0)$ or $K^+K^-\pi^+\pi^-$, as shown in Fig. 1, an unbinned maximum likelihood fit is performed to the corresponding mass spectrum. In each fit, the signal is described with the MC simulated shape convolving with a Gaussian function, and the background is described with an ARGUS function [18], except for the mode $h_c \rightarrow K^+K^-\pi^+\pi^-$ where an additional

TABLE I. The corresponding results for each decay mode. Mode I, II, III, IV, and V represent the decay modes $\psi(3686) \rightarrow \pi^0 h_c$ with $h_c \rightarrow p\bar{p}\pi^+\pi^-$, $\pi^+\pi^-\pi^0$, $2(\pi^+\pi^-)\pi^0$, $3(\pi^+\pi^-)\pi^0$, and $K^+K^-\pi^+\pi^-$, respectively, ϵ represents the selection efficiency, N_{h_c} represents the h_c signal yield, $\mathcal{B}_{\psi(3686)}$ and \mathcal{B}_{h_c} represents the branching fraction $\mathcal{B}(\psi(3686) \rightarrow \pi^0 h_c)$ and $\mathcal{B}(h_c \rightarrow \text{hadrons})$, S.S. is the statistical significance, and $\mathcal{B}_{h_c}^{\text{PDG}}$ represents the branching fraction of $h_c \rightarrow \text{hadrons}$ from PDG [6]. Only statistical uncertainties are presented for signal yields, while the first uncertainties are statistical and the second ones systematic for the (product) branching fractions. For decay mode $h_c \rightarrow 3(\pi^+\pi^-)\pi^0$ especially, both branching fraction and upper limit are listed.

Mode	$\epsilon(\%)$	N_{h_c}	$\mathcal{B}_{\psi(3686)} \times \mathcal{B}_{h_c}(10^{-6})$	$\mathcal{B}_{h_c}(10^{-3})$	S.S.	$\mathcal{B}_{h_c}^{\text{PDG}}(10^{-3})$
I	20.9	230 ± 25	$2.49 \pm 0.27 \pm 0.29$	$2.89 \pm 0.32 \pm 0.55$	7.4σ	—
II	16.8	101 ± 25	$1.38 \pm 0.35 \pm 0.18$	$1.60 \pm 0.40 \pm 0.32$	4.9σ	< 2.2
III	9.1	254 ± 32	$6.40 \pm 0.81 \pm 0.93$	$7.44 \pm 0.94 \pm 1.56$	9.1σ	22^{+8}_{-7}
IV	4.2	73 ± 34	$4.00 \pm 1.87 \pm 0.73$	$4.65 \pm 2.17 \pm 1.10$	2.1σ	< 29
		< 136	< 7.5	< 8.7	—	—
V	18.1	< 40	< 0.5	< 0.6	—	—

background component from $\psi(3686) \rightarrow \gamma\chi_{c2}$ ($\chi_{c2} \rightarrow K^+K^-\pi^+\pi^-$) is included. Here, the MC shape includes intrinsic h_c line shape and detection resolution, while the Gaussian function accounts for the resolution discrepancy between data and MC simulation. All the parameters of the Gaussian and ARGUS functions, except the threshold $3.551 \text{ GeV}/c^2$, are floated in the fit.

Branching fractions are calculated based on the formula,

$$\mathcal{B}_{h_c} = \frac{N_{h_c}}{\mathcal{B}(\psi(3686) \rightarrow \pi^0 h_c) \cdot \mathcal{B}(\pi^0 \rightarrow \gamma\gamma) \cdot N_{\psi(3686)} \cdot \epsilon}, \quad (1)$$

where \mathcal{B}_{h_c} represents the branching fraction of $h_c \rightarrow p\bar{p}\pi^+\pi^-$, $\pi^+\pi^-\pi^0$, $2(\pi^+\pi^-)\pi^0$, $3(\pi^+\pi^-)\pi^0$ or $K^+K^-\pi^+\pi^-$, while $\mathcal{B}(\psi(3686) \rightarrow \pi^0 h_c)$ and $\mathcal{B}(\pi^0 \rightarrow \gamma\gamma)$ are the branching fractions of $\psi(3686) \rightarrow \pi^0 h_c$ and $\pi^0 \rightarrow \gamma\gamma$, respectively, N_{h_c} and $N_{\psi(3686)}$ are the numbers of h_c signal and $\psi(3686)$ events, respectively, ϵ is the selection efficiency obtained from signal MC simulation. Since no significant signal is observed in decays $h_c \rightarrow K^+K^-\pi^+\pi^-$ and $3(\pi^+\pi^-)\pi^0$, their upper limits are determined with the Bayesian method [19]. With the fit function described before, we scan the number of signal yield to obtain the likelihood distribution, and smear it with the systematic uncertainties. The upper limits of the number of signal yield $N_{h_c}^{up}$ at 90% confidence level is obtained via $\int_0^{N_{h_c}^{up}} F(x)dx / \int_0^\infty F(x)dx = 0.90$, where $F(x)$ is the probability density function of the likelihood distribution. All the numerical results, including selection efficiencies, signal yields, branching fractions or upper limits and statistical significances, are listed in Table I.

The sources of systematic uncertainties for the product branching fractions of $\psi(3686) \rightarrow$

TABLE II. The relative uncertainties for each decay mode (in %). I, II, III, IV, and V represent the decay modes $\psi(3686) \rightarrow \pi^0 h_c$ with $h_c \rightarrow p\bar{p}\pi^+\pi^-$, $\pi^+\pi^-\pi^0$, $2(\pi^+\pi^-)\pi^0$, $3(\pi^+\pi^-)\pi^0$, and $K^+K^-\pi^+\pi^-$, respectively.

Source	I	II	III	IV	V
Tracking	5.0	2.0	4.0	6.0	4.0
Photon	2.0	4.0	4.0	4.0	2.0
π^0 reconstruction	1.0	2.0	2.0	2.0	1.0
PID	4.9	2.0	4.0	6.0	4.0
Kinematic fit	1.8	2.2	3.7	4.2	1.5
Number of $\psi(3686)$	0.7	0.7	0.7	0.7	0.7
Fitting range	2.6	3.5	4.9	—	—
Signal shape	1.3	8.1	2.5	—	—
Background shape	2.1	3.5	2.9	—	—
Resolution	4.2	5.1	3.3	—	—
η_c	—	—	1.5	—	—
Mass windows	1.9	4.0	5.0	5.0	1.0
Physics model	6.4	3.2	8.3	14.1	7.4
Sum	11.5	13.3	14.6	18.3	9.8

$\pi^0 h_c$ and $h_c \rightarrow p\bar{p}\pi^+\pi^-$, $\pi^+\pi^-\pi^0$, $2(\pi^+\pi^-)\pi^0$, $3(\pi^+\pi^-)\pi^0$, or $K^+K^-\pi^+\pi^-$ include tracking, photon and π^0 reconstruction, PID, kinematic fit, number of $\psi(3686)$ events, fitting procedure, η_c peaking background, mass windows and the physics model describing the h_c production and decay dynamics. All the systematic uncertainties are summarized in Table II, and the overall systematic uncertainties are obtained by summing all individual ones in quadrature. In addition, we add a relative systematic uncertainty of 15.2% from branching fraction of $\psi(3686) \rightarrow \pi^0 h_c$ in calculating the branching fraction of h_c hadronic decays.

The uncertainties of tracking efficiency are estimated with the control samples $\psi(3686) \rightarrow \pi^+\pi^- J/\psi$, $J/\psi \rightarrow K_S^0 K^\pm \pi^\mp$ and $\psi(3686) \rightarrow p\bar{p}\pi^+\pi^-$, and are determined to be 1.0% [20], 1.0% [21], 1.3%, and 1.7% for each charged pion, kaon, proton, and anti-proton, respectively. The uncertainties of photon and π^0 reconstruction efficiency are studied using control sample $J/\psi \rightarrow \pi^+\pi^-\pi^0$, and are quoted as 1.0% per photon [22] and 1% per π^0 [22]. The uncertainties of PID are determined to be 1.0% per pion [23], 1.0% per kaon [21], 1.3% per proton and 1.6% per antiproton based on the control samples used to estimate tracking uncertainty. The uncertainty associated with the kinematic fit is estimated by comparing the efficiencies with and without the helix parameter correction [24]. The uncertainty of the number of $\psi(3686)$ events is 0.7% according to the study in Ref. [9].

Fitting range, signal shape, background shape and resolution difference between data and MC

simulation are considered as the individual sources of the systematic uncertainties related to the fitting procedure, and are estimated by varying the fitting ranges ($\pm 10 \text{ MeV}/c^2$ on boundaries), the signal shape (MC shape is replaced with a Breit-Wigner function) and the background shape (the ARGUS function is replaced with a second-order Chebychev function) correspondingly. The difference between the results obtained by fixing and releasing the resolution is taken as the uncertainty of the resolution difference between data and MC simulation. The fixed resolution difference is determined as $1 \text{ MeV}/c^2$, obtained with control sample $\psi(3686) \rightarrow \gamma \chi_{c1} \rightarrow \gamma p \bar{p} \pi^+ \pi^-$. For $h_c \rightarrow 3(\pi^+ \pi^-) \pi^0$ and $K^+ K^- \pi^+ \pi^-$, the largest upper limits are taken with different combinations of fitting models and ranges. The uncertainty due to η_c peaking background comes from the number of η_c events whose statistical and systematic uncertainties have been estimated based on its fit and measured branching fractions, respectively. The uncertainty due to the mass windows in background veto is estimated by enlarging or reducing their ranges, and the largest difference is taken as systematic uncertainty.

The systematic uncertainties due to physics model come from two sources, intermediate states in h_c decays and the h_c angular distribution in $\psi(3686) \rightarrow \pi^0 h_c$. We search for the intermediate states for $h_c \rightarrow p \bar{p} \pi^+ \pi^-$, $\pi^+ \pi^- \pi^0$, and $2(\pi^+ \pi^-) \pi^0$ in our data. The invariant mass spectra of possible combinations with the final states are shown in Figs. 2, 3, and 4 for $h_c \rightarrow p \bar{p} \pi^+ \pi^-$, $\pi^+ \pi^- \pi^0$, and $2(\pi^+ \pi^-) \pi^0$, respectively. In each figure, the background has been subtracted with the h_c sideband $|RM(\pi_l^0) - 3.542| < 0.004 \text{ GeV}/c^2$ and $|RM(\pi_l^0) - 3.508| < 0.004 \text{ GeV}/c^2$. In spite of large statistical fluctuations, we find some possible intermediate states, such as a ρ^0 peak in each projection of the $\pi^+ \pi^-$ invariant mass. They are estimated by generating alternative MC samples with possible resonances or specific angular distributions of h_c in $\psi(3686) \rightarrow \pi^0 h_c$, and the largest difference between the efficiencies of the nominal MC and the other MC samples is taken.

In summary, three h_c hadronic decays, $h_c \rightarrow p \bar{p} \pi^+ \pi^-$, $h_c \rightarrow \pi^+ \pi^- \pi^0$, and $h_c \rightarrow 2(\pi^+ \pi^-) \pi^0$, are observed for the first time, and two channels, $h_c \rightarrow K^+ K^- \pi^+ \pi^-$ and $h_c \rightarrow 3(\pi^+ \pi^-) \pi^0$, are searched for. The measured branching fractions or upper limits, as well as their statistical significance, are listed in Table I. The measured branching fraction of $h_c \rightarrow 2(\pi^+ \pi^-) \pi^0$ is obviously smaller and more precise than CLEO-c result [7], although they are consistent within uncertainties. The sum of the branching fractions of the three observed channels is approximately 1.2%, which is still obviously smaller than the h_c radiative transition to the η_c . It is difficult to conclude the expectation, the total hadronic decay width of the h_c is likely of the same order as its radiative

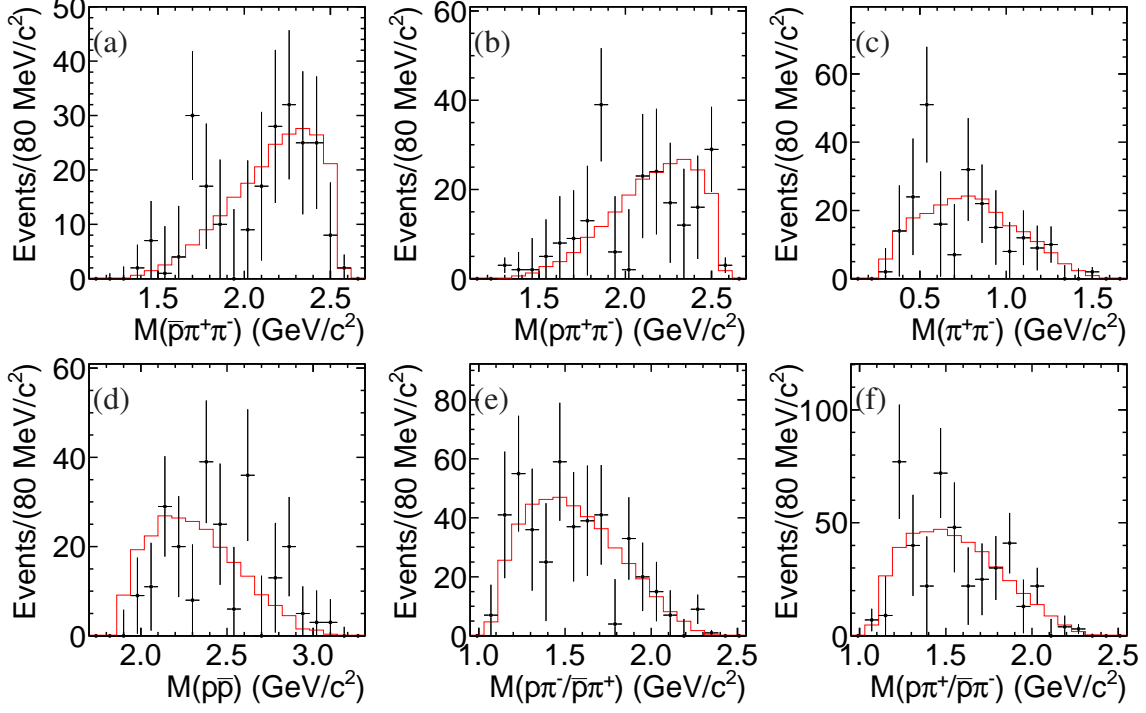


FIG. 2. The invariant mass spectra of (a) $\bar{p}\pi^+\pi^-$, (b) $p\pi^+\pi^-$, (c) $\pi^+\pi^-$, (d) $p\bar{p}$, (e) $p\pi^-/\bar{p}\pi^+$, and (f) $p\pi^+/\bar{p}\pi^-$ for decay mode $h_c \rightarrow p\bar{p}\pi^+\pi^-$. In each spectra, the dots are data subtracted sideband background, the red histogram is the PHSP signal MC (color online).

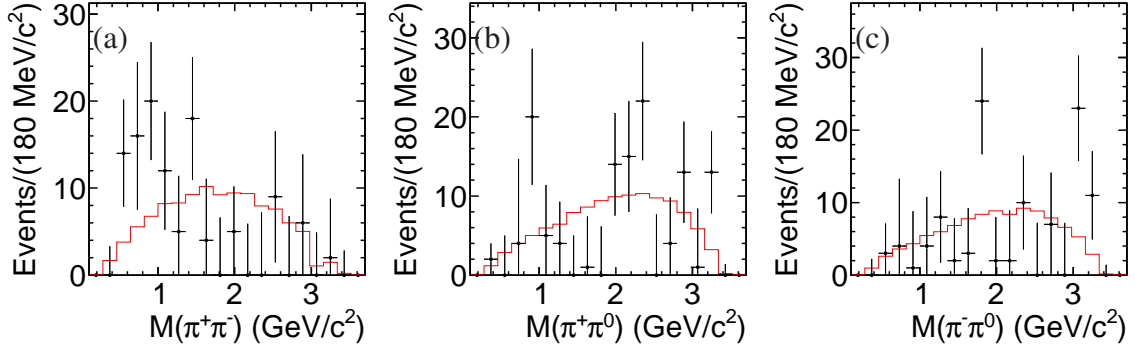


FIG. 3. The invariant mass spectra of (a) $\pi^+\pi^-$, (b) $\pi^+\pi^0$, and (c) $\pi^-\pi^0$ for decay mode $h_c \rightarrow \pi^+\pi^-\pi^0$. In each spectra, the dots are data subtracted sideband background, the red histogram is the PHSP signal MC (color online).

transition, is correct. So, measurements of more h_c hadronic decay modes should be helpful to clarify this problem. Table III shows the comparisons of the ratios of the hadronic decay widths $\Gamma_{h_c}^{\text{had}}/\Gamma_{\eta_c}^{\text{had}}$ and $\Gamma_{h_c}^{\text{had}}/\Gamma_{J/\psi}^{\text{had}}$ between theoretical predictions and experimental measurements. Here the factors associated with exclusive modes such as multiplicity and phase space are ignored. The results based on pQCD are obviously smaller than that based on NRQCD, and pQCD is favored by the small experimental results measured in this analysis. However, in Ref. [8], the theoret-

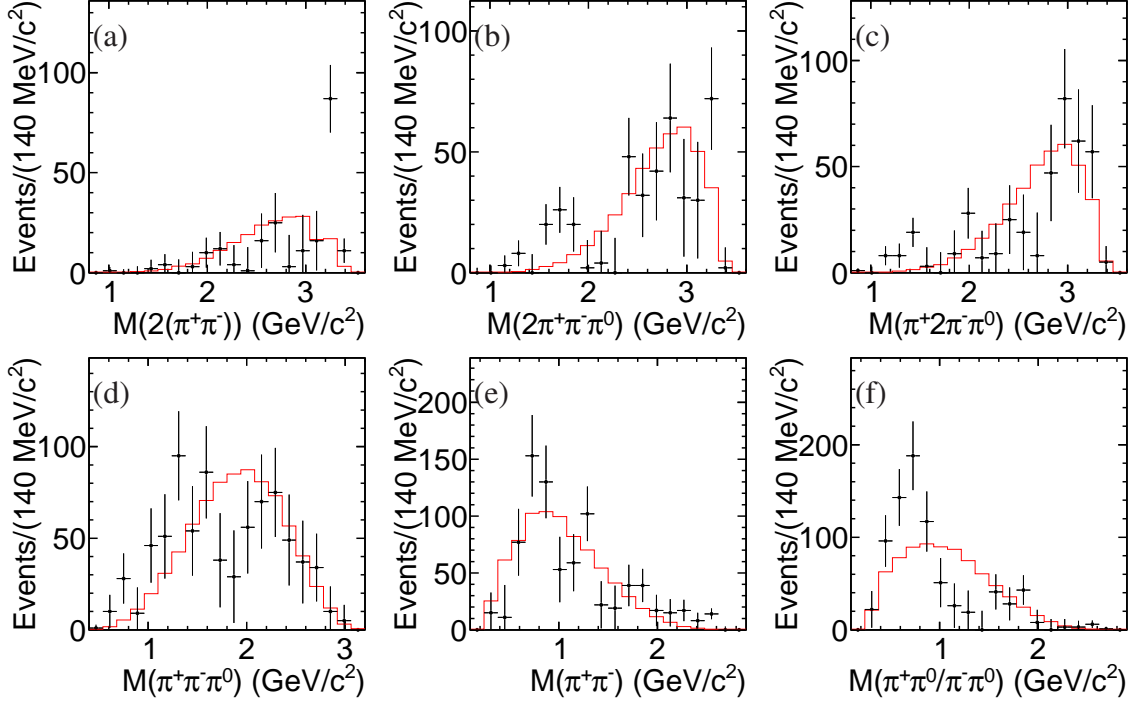


FIG. 4. The invariant mass spectra of (a) $2(\pi^+\pi^-)$, (b) $2\pi^+\pi^-\pi^0$, (c) $\pi^+2\pi^-\pi^0$, (d) $\pi^+\pi^-\pi^0$, (e) $\pi^+\pi^-$, and (f) $\pi^+\pi^0/\pi^-\pi^0$ for decay mode $h_c \rightarrow 2(\pi^+\pi^-)\pi^0$. In each spectra, the dots are data subtracted sideband background, the red histogram is PHSP signal MC (color online).

TABLE III. The ratios of the hadronic decay widths of h_c to η_c ($\Gamma_{h_c}^{\text{had}}/\Gamma_{\eta_c}^{\text{had}}$) and h_c to J/ψ ($\Gamma_{h_c}^{\text{had}}/\Gamma_{J/\psi}^{\text{had}}$). The theoretical predictions of the total hadronic decay ratios are based on pQCD and NRQCD [8], which are expected to be correct also for exclusive decay modes. The experimental measurements of the ratios of the partial decay widths for $p\bar{p}\pi^+\pi^-$, $K^+K^-\pi^+\pi^-$, and $n(\pi^+\pi^-)\pi^0$ ($n = 0, 1, 2$) modes are calculated based on the measured branching fractions in this analysis and PDG [6], while the factors associated with exclusive modes such as multiplicity and phase space are ignored.

	Model/Mode	Ratio
$\Gamma_{h_c}^{\text{had}}/\Gamma_{\eta_c}^{\text{had}}$	pQCD	0.010 ± 0.001
	NRQCD	0.083 ± 0.018
	$p\bar{p}\pi^+\pi^-$	0.012 ± 0.008
	$K^+K^-\pi^+\pi^-$	< 0.083
$\Gamma_{h_c}^{\text{had}}/\Gamma_{J/\psi}^{\text{had}}$	pQCD	0.68 ± 0.07
	NRQCD	8.03 ± 1.31
	$p\bar{p}\pi^+\pi^-$	3.63 ± 2.25
	$\pi^+\pi^-\pi^0$	0.57 ± 0.38
	$2(\pi^+\pi^-)\pi^0$	1.43 ± 0.90
	$3(\pi^+\pi^-)\pi^0$	< 2.26
	$K^+K^-\pi^+\pi^-$	< 0.68

cal prediction of $\mathcal{B}(h_c \rightarrow \gamma\eta_c) = (41 \pm 3)\%$ based on NRQCD is favored by the experimental measurement $(51 \pm 6)\%$ [6], compared with $(88 \pm 2)\%$ based on pQCD. We notice that the experimental measurements are still limited to low statistics and the original theoretical models can be modified with some considerations such as normalization scale or relativistic correction [25, 26]. Improvements on the experimental measurements and theoretical calculations in the future are expected to understand this inconsistency.

The BESIII collaboration thanks the staff of BEPCII and the IHEP computing center for their strong support. This work is supported in part by National Key Basic Research Program of China under Contract No. 2015CB856700; National Natural Science Foundation of China (NSFC) under Contracts Nos. 11335008, 11425524, 11625523, 11635010, 11735014, 11565006; the Chinese Academy of Sciences (CAS) Large-Scale Scientific Facility Program; the CAS Center for Excellence in Particle Physics (CCEPP); Joint Large-Scale Scientific Facility Funds of the NSFC and CAS under Contracts Nos. U1532257, U1532258, U1732263; CAS Key Research Program of Frontier Sciences under Contracts Nos. QYZDJ-SSW-SLH003, QYZDJ-SSW-SLH040; 100 Talents Program of CAS; INPAC and Shanghai Key Laboratory for Particle Physics and Cosmology; German Research Foundation DFG under Contracts Nos. Collaborative Research Center CRC 1044, FOR 2359; Istituto Nazionale di Fisica Nucleare, Italy; Koninklijke Nederlandse Akademie van Wetenschappen (KNAW) under Contract No. 530-4CDP03; Ministry of Development of Turkey under Contract No. DPT2006K-120470; National Science and Technology fund; The Swedish Research Council; U. S. Department of Energy under Contracts Nos. DE-FG02-05ER41374, DE-SC-0010118, DE-SC-0010504, DE-SC-0012069; University of Groningen (RuG) and the Helmholtzzentrum fuer Schwerionenforschung GmbH (GSI), Darmstadt.

-
- [1] P. Rubin *et al.* [CLEO Collaboration], Phys. Rev. D **72**, 092004 (2005).
 - [2] J. L. Rosner *et al.* [CLEO Collaboration], Phys. Rev. Lett. **95**, 102003 (2005).
 - [3] M. Andreotti *et al.* [Fermilab E835 Collaboration], Phys. Rev. D **72**, 032001 (2005).
 - [4] S. Dobbs *et al.* [CLEO Collaboration], Phys. Rev. Lett. **101**, 182003 (2008).
 - [5] M. Ablikim *et al.* [BESIII Collaboration], Phys. Rev. Lett. **104**, 132002 (2010).
 - [6] M. Tanabashi *et al.* [Particle Data Group], Phys. Rev. D **98**, 030001 (2018).
 - [7] G. S. Adams *et al.* [CLEO Collaboration], Phys. Rev. D **80**, 051106 (2009).

- [8] Y. P. Kuang, Phys. Rev. D **65**, 094024 (2002).
- [9] M. Ablikim *et al.* [BESIII Collaboration], Chin. Phys. C **42**, 023001 (2018).
- [10] M. Ablikim *et al.* [BESIII Collaboration], Nucl. Instrum. Meth. A **614**, 345 (2010).
- [11] S. Jadach, B. F. L. Ward and Z. Was, Comput. Phys. Commun. **130**, 260 (2000).
- [12] S. Jadach, B. F. L. Ward and Z. Was, Phys. Rev. D **63**, 113009 (2001).
- [13] R. G. Ping, Chin. Phys. C **32**, 599 (2008).
- [14] J. C. Chen, G. S. Huang, X. R. Qi, D. H. Zhang and Y. S. Zhu, Phys. Rev. D **62**, 034003 (2000).
- [15] S. Agostinelli *et al.* [GEANT4 Collaboration], Nucl. Instrum. Meth. A **506**, 250 (2003).
- [16] J. Allison *et al.*, IEEE Trans. Nucl. Sci. **53**, 270 (2006).
- [17] Z. Y. Deng *et al.*, HEP & NP **30**, 371 (2006).
- [18] H. Albrecht *et al.* [ARGUS Collaboration], Phys. Lett. B **340**, 217 (1994).
- [19] G. J. Feldman, R. D. Cousins, Phys. Rev. D **57**, 3873 (1998).
- [20] M. Ablikim *et al.* [BESIII Collaboration], Phys. Rev. Lett. **105**, 261801 (2010).
- [21] M. Ablikim *et al.* [BESIII Collaboration], Phys. Rev. D **83**, 112005 (2011).
- [22] M. Ablikim *et al.* [BESIII Collaboration], Phys. Rev. D **81**, 052005 (2010).
- [23] M. Ablikim *et al.* [BESIII Collaboration], Phys. Rev. D **86**, 092009 (2012).
- [24] M. Ablikim *et al.* [BESIII Collaboration], Phys. Rev. D **87**, 012002 (2013).
- [25] Q. L. Zhang, X. G. Wu, X. C. Zheng, S. Q. Wang, H. B. Fu and Z. Y. Fang, Chin. Phys. Lett. **31**, 051202 (2014).
- [26] J. Z. Li, Y. Q. Ma and K. T. Chao, Phys. Rev. D **88**, 034002 (2013).